DETECTION OF RENAL CELL CARCINOMA USING NEUTRON TIME OF FLIGHT SPECTROSCOPY

Rodrigo S Viana[1], Manu N Lakshmanan[2], Greeshma A Agasthya[2], Hélio Yoriyaz[1], Anuj J Kapadia[2]

[1]Instituto de Pesquisas Energéticas e Nucleares (IPEN / CNEN - SP)
Av. Professor Lineu Prestes 2242
05508-000 São Paulo, SP
rodrigossviana@gmail.com

[2]Ravin Advanced Imaging Labs, Radiology
Duke University Medical Center
Durham, NC 27710, USA

ABSTRACT

The diagnosis of renal cell carcinoma (RCC) is challenging because the symptoms accompanying it are not unique to the disease, and can therefore be misdiagnosed as other diseases. Due to this characteristic, detection of renal cancer is incidental most of time, occurring via abdominal radiographic examinations unrelated to the disease. Presently, biopsy, which is invasive and an unpleasant procedure for the patient, is the most commonly used technique to diagnose RCC. In this study, we demonstrate the application of a novel noninvasive technique for detecting and imaging RCC *in vivo*. The elemental composition of biological tissues including kidneys has been investigated using a new technique called Neutron Stimulated Emission Computed Tomography (NSECT). This technique is based on detecting the energy signature emitted by the stable isotopes of elements in the body, which are stimulated to emit gamma radiation via inelastic neutron scattering. Methods for improving detection sensitivity and reducing dose, such as time-of-flight neutron spectroscopy have been explored. MCNP5 simulations were used to model the NSECT scanning of the human kidney where the energy and time of arrival of gamma photons were recorded in an ideal detector placed around the human torso. A 5 MeV collimated neutron beam was used to irradiate the kidney containing an RCC lesion. The resulting spectra were resolved in 100 picosecond and 1 keV time and energy bins, respectively. The preliminary results demonstrate the ability to localize the lesion through neutron time of flight spectroscopy and generate a tomographic image at a low dose to the patient.

1. INTRODUCTION

Renal cancer is one of the ten most common cancers in both genders according to the American Cancer Society [1]. The diagnosis of such a disease is difficult because the patient can present symptoms common to other diseases or can be even asymptomatic. In most cases, the lesion of renal cancer is detected incidentally due to other abdominal examinations conducted for various health conditions. As a complementary approach to medical imaging, biopsy still remains the most used and reliable technique for detection of renal cell carcinoma (RCC) [2-5] despite being an invasive procedure.

Floyd et al. [6] presented a new technique called Neutron Stimulated Emission Computed Tomography (NSECT), a noninvasive tomographic imaging method for measuring elements in the body. NSECT is based on inelastic neutron scattering between incident fast neutrons and stable nuclei in the body composition. This leads to the emission of gamma photons. The energy of the emitted gamma photon is intrinsic to the emitting nucleus and can be used to identify the elemental composition of the irradiated tissue. Hence, NSECT can be used to detect and quantify the elements that are present in the human body as well as differentiate healthy tissue from tumors without the need for any tracers or injections.

Since each isotope emits photons with particular energies, tomographic reconstructions can be performed from sinograms of each element of interest, which requires a set of neutron beam projections around the tissue. Depending on the number of neutron beam projections required for image reconstruction, the dose to the patient from NSECT can be high, rendering the scan unfeasible.

In order to reduce the dose deposition, Agasthya et al. [7] presented the first results from a new technique based on the neutron time-of-flight (TOF) information associated with the photon emission spectrum. Given a monochromatic beam, the neutron velocity of the incident neutrons can be determined. This velocity can be associated with the time of arrival of those photons emitted from inelastic scattering processes. The photon emission spectrum contains information about the tissue composition through the energy peaks but the element location along the neutron beam path is unknown. Once the time of detection (time between incidence of neutron and detection of photon) for the emitted photons are recorded; the element location can be calculated along the neutron beam path through the linear relationship of neutron velocity with time of detection. From these time resolved spectra corresponding to a set of single angle neutron beam translations a tomographic image can be generated.

In this paper, we propose the application of the neutron TOF spectroscopy as a non-invasive technique to detect renal cancer *in vivo* and differentiate between healthy and malignant kidney tissue. A TOF-based NSECT scan was simulated with the MCNP5 code using an adult tomographic phantom containing the kidney composition for renal cell carcinoma (RCC) and healthy tissue.

2. METHODOLOGY

In this section we describe the Monte Carlo simulations performed using MCNP5 [8] code to model the NSECT scan, and the procedures for dose calculation, data acquisition and analysis for neutron TOF spectroscopy.

2.1. MCNP5 simulation

The NSECT scan simulated in this work uses perfect gamma-ray detectors, a neutron source and an anatomical phantom as described below.

Neutron source: The neutron source was modeled to emit a collimated 5-MeV neutron beam with a square cross-section of area 1 cm^2. The beam energy was chosen in order to stimulate high energies such as the 4.439 MeV level in ^{12}C.

Gamma-ray detectors: The modeled detection system consisted of six cylinders with 100% detection efficiency, set up around the anatomical phantom in two semi circles of 22 cm radius (Figure 1a-b). Each semi circle arrangement contains 3 detectors angled at 30° from each other and with respect to the *x*-axis. A 3 cm gap was left between the two semi-circular rows of detectors to allow the neutron beam to pass. Each detector was modeled as a cylinder of 10 cm diameter and 10 cm height. The signal detected across detectors was summed for spectra and image acquisition.
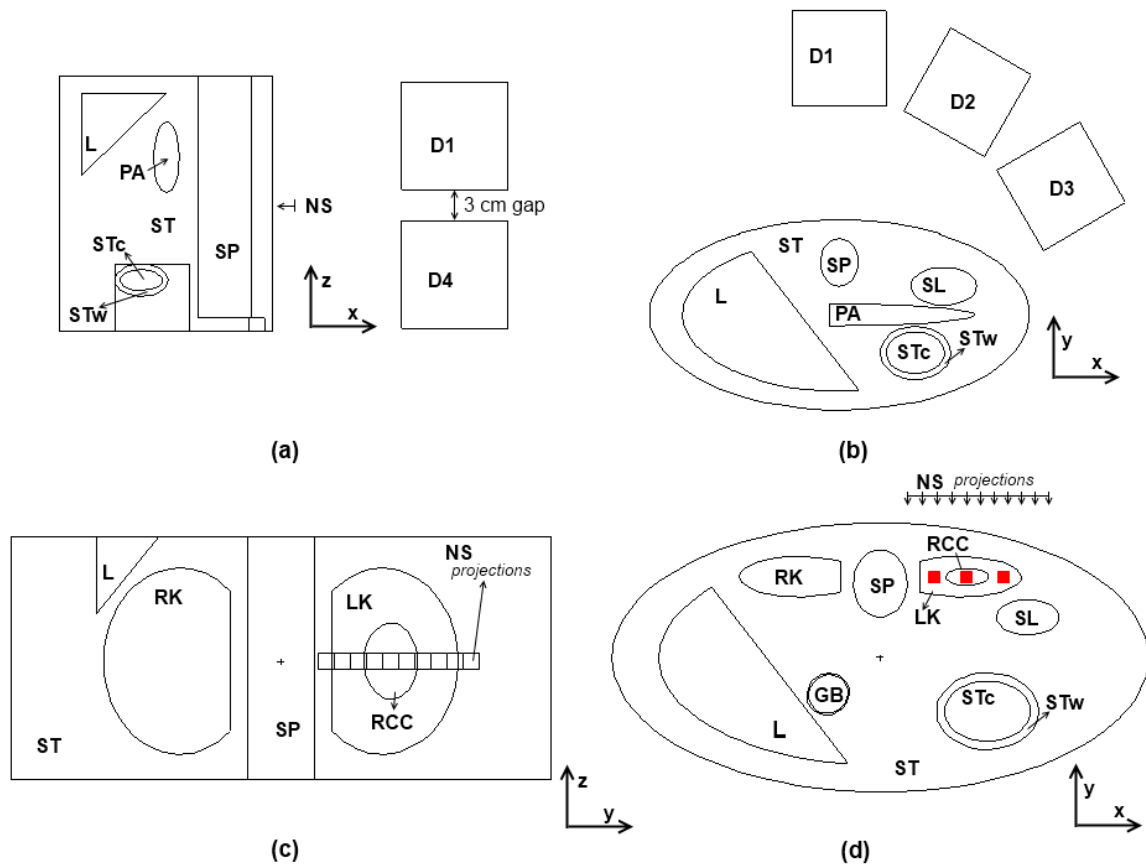

Figure 1. The 2D views of the detection system and anatomical phantom. (a-b) Sagittal and transverse views of phantom surrounded by a set of detectors. Only four of the six detectors can be seen in these views (D1-D4). 'NS' represents the neutron source firing the beam at different projections, which are shown in (c-d). Labels are provided for tissue identification: L - liver, GB - gallbladder, SP - spine, SL - spleen, STw - stomach wall, STc - stomach contents, ST - soft tissue, LK - left kidney, RK - right kidney, PA - pancreas and RCC – renal cell carcinoma. The three red squares in (d) indicate the regions of interest (ROIs) used in image analysis.

Anatomical phantom: The phantom adopted in this work is the mathematical phantom developed by Cristy and Eckerman [9]. The organs in the phantom as well as the material composition correspond to an adult male. The RCC lesion was modeled as an ellipsoid of 3.16 x 1.26 x 4.46 cm located in the centre of the left kidney (Figure 1c-d).

The material composition of each organ was set based on the ICRU 46 [10] and ICRP 103 [11] reports. The composition of the RCC lesion was modeled by changing the elemental concentrations of the ICRU 46 [10] renal tissue to reflect the elemental changes according to a published clinical study described by Calvo et al. [12] (shown in Table 1). The anatomical phantom was surrounded by vacuum.

Table 1: Material composition for RCC and healthy kidney used in the Monte-Carlo modeling. Both tissues were modeled using the density 1.05 g/cm^3.

Element	RCC lesion (% mass fraction)	Healthy Kidney (% mass fraction)
Al	8.10E-04	4.60E-06
C	1.33E+01	1.30E+01
Ca	5.10E-02	3.30E-02
Cd	2.30E-04	1.40E-03
Cl	2.00E-01	2.00E-01
Cr	1.30E-04	5.00E-07
Cu	8.00E-04	8.30E-04
Fe	2.50E-02	3.20E-02
H	1.03E+01	1.02E+01
K	5.00E-03	1.60E-02
Mg	6.60E-03	9.90E-03
Mn	9.80E-05	9.20E-05
N	3.00E+00	3.00E+00
Na	1.00E-02	1.60E+00
O	7.28E+01	7.16E+01
P	6.30E-02	4.30E-03
Pb	1.70E-04	5.00E-06
S	2.00E-01	2.00E-01
Zn	2.50E-02	7.00E-06

2.2. Spectra and image acquisition

The collimated neutron beam was translated in 10 non-overlapping steps, illuminating the central section of the left kidney, as exemplified in Figure 1c. The beam positions were set in order to irradiate both healthy and tumor tissue.

The photon fluence spectra were recorded in 1-keV energy bins at the detectors for each beam position. In order to decrease the statistical error, the photon spectra recorded at those detectors placed at the same angle with respect to x axis were summed, e.g., the photon spectra recorded at detectors D1 and D4 in Figure 1a were summed. In association with the photon spectra, each pair of detectors also reported the time of arrival of each gamma photon in 100-ps time bins.

The velocity and kinetic energy of the neutron are related according to the expression $E = \frac{mv^2}{2}$, where m and v are the mass and velocity of the neutron, respectively. For example, assuming the energy of the neutron beam was set to 5 MeV, the neutron velocity can be calculated as approximately 3.09×10^7 m/s. Therefore, a 5 MeV neutron can travel along 1 cm distance in about 0.32 ns. Then the time of detection of the gamma photon can be related to the depth location of the neutron inelastic scatter using the neutron velocity [7].

According to the material composition shown in Table 1, one of the elements that can be used to distinguish the RCC lesion from healthy kidney tissue is sodium, since there is a factor of 160 between the mass fractions of this element in RCC and healthy kidney tissues. Based on

this composition, the time-resolved spectrum for photons detected in the 0.439 MeV energy bin, which corresponds to one of the energy levels in ^{23}Na, was recorded for each neutron beam translation. In addition, the time-resolved spectrum for the energy 4.439 MeV from ^{12}C was also acquired in order to establish the kidney location regardless the presence of lesion.

The recorded time-resolved spectrum for each element was associated with the positions from the neutron beam translations. Then, tomographic images representing the spatial location of the elements of interest (^{23}Na and ^{12}C) were acquired by converting the time-based spectra into depth locations. As a result, the pixel's image is proportional to the concentration of the element. All images were corrected for neutron attenuation according to the methodology described in Kapadia and Floyd [13].

2.3. Image analysis

Three regions of interest (ROIs) were selected, in the ^{23}Na image, at the depth corresponding to the RCC lesion. One ROI in the lesion and two on either side of the lesion in the healthy kidney, as indicated in Figure 1d. The average value of the gray levels for both ROIs were compared using the Student's t-test for difference of means. As a primary study, the difference of composition was assumed only for a two-tailed p-value ≤ 0.05 (95% confidence level).

For the purpose of visualization, a combination of ^{23}Na and ^{12}C images through superimposition was displayed in order to correlate the chemical information from the kidneys composition with the anatomy of the irradiated organs. The element ^{12}C was chosen for this image superimposition because is a common element among organs and is present in human body in high concentration.

2.4. Dose calculation

The average effective dose associated with the 10 neutron beam translations was calculated considering the coupled transport of photons, neutrons and electrons based on a source intensity of 1.5×10^7 for each neutron beam translation [7].

3. RESULTS AND DISCUSSION

3.1. Image acquisition and lesion location

The results shown by Agasthya et al. [7] point out the feasibility of the TOF-based NSECT scan for locating the depth of iron lesions using a single neutron beam projection. The same concept was applied in this work using 10 neutron beam projections illuminating 10 cm of adult kidney, as exemplified in Figure 1c,d. For each neutron beam translation, a time-resolved spectrum was acquired for the energies 4.439 MeV and 0.439 MeV respectively from ^{12}C and ^{23}Na. The time-resolved spectra for both elements were organized according to the displacement of the neutron beam translations. From this procedure, two matrices were acquired, one for ^{12}C and one for ^{23}Na, whose columns are related with the time of arrival of the emitted photons (ns) and whose rows are related to the translation position where the neutron beam was projected (cm). Then the conversion from time to space-resolved axis was performed using the velocity for 5 MeV neutrons (3.09×10^7 m/s).

3.2. Statistical analysis

Quantitative analysis was performed on [23]Na image for the left kidney considering three ROIs within the kidney only: left side of the healthy kidney (LSK) close to the spine, middle of the RCC lesion (L) and right side of the healthy kidney (RSK). Each ROI was evaluated at the same depth and with the same number of pixels.

The mean pixel value as well as the standard deviation for each ROI were compared to evaluate the ratios among both sides of the healthy kidney with the RCC lesion, i.e. (RSK:L) and (LSK:L). Statistical comparisons were performed using a two-tailed t-test for difference of means with p-value $\leq$ 0.05 (95% confidence level). Table 2 summarizes the findings for the quantitative analysis of [23]Na image.

Table 2: Quantitative analysis for difference of mean pixel value within the kidney.

Element	ROI	μ	σ	ROIs	p-value	Evaluated ratio
23Na (0.439 MeV)	LsK	0.9419	0.0524	LsK:L	$<1\ 10^{-16}$	2.4732 (LsK/L)
	L	0.3333	0.0840	RsK:L	$<1\ 10^{-14}$	2.8264 (RsK/L)
	RsK	0.8242	0.0308			

As shown in Table 2, the mean pixel values from RSK:L and LSK:L were found to be statistically different from each other. The ratios of the mean pixel value across the three ROIs (LsK/L and RsK/L) were found to be in general agreement with the expected increase/decrease trend between the healthy kidney and RCC lesion, i.e. the concentration of [23]Na is higher in healthy kidney than in the RCC lesion.

The difference observed from the comparison of the evaluated ratios LsK/L and RsK/L and the expected ratio based on the material composition described on Table 1 can be explained based on the sensitivity of detection of the NSECT system. [23]Na is present in soft tissue, healthy kidney and in the RCC lesion respectively in 0.1%, 0.01% and 1.6%. These are low concentrations and very different among each other; however, due to the sensitivity of NSECT scan, we may not be able to quantify accurately the concentration of [23]Na due to photon scattering among tissues at the same depth. This effect doesn't make visible the linearity between the element concentration and the signal from the detected photons. According to Agasthya et al. [14], patient size, the number of detectors and the concentration of element itself are decisive factors to the sensitivity of detection for NSECT scan.

3.3. Image superimposition

In order to correlate the anatomical information of the irradiated tissues with the chemical composition of the RCC lesion, the images from ^{12}C and [23]Na were superimposed, as shown in Figure 2c. The ^{12}C image (Figure 2a) shows the contour of the torso, the left kidney, spleen and stomach, exactly as described in Figure 1d. The [23]Na image must highlight the kidney's location due to the high concentration of this element among other organs as well as the RCC lesion. Therefore, when the information from ^{12}C and [23]Na are combined, we are able to identify the general anatomy of the irradiated tissues and the RCC lesion as well; which can be identified by the lack of [23]Na within the kidney in Figure 2b,c.
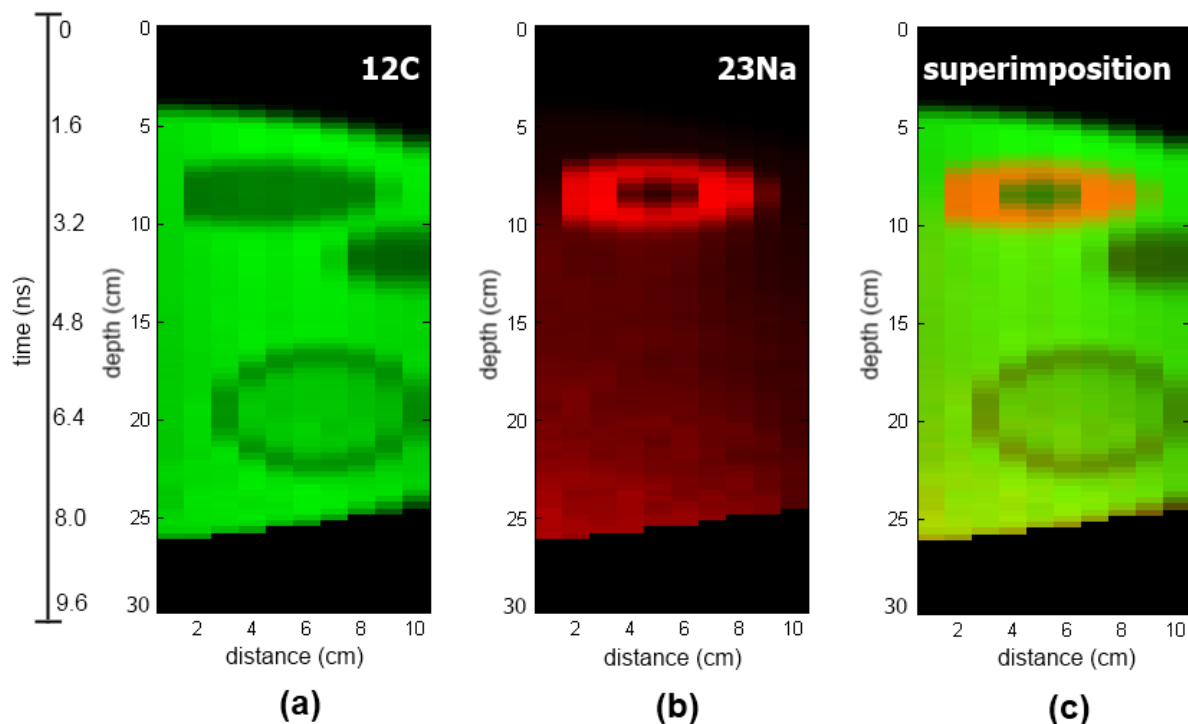
Figure 2. Images from 12C (a) and 23Na (b) employed in the image superimposition (c).

3.4. Dosimetry

The irradiation protocol used in this work comprises of 10 neutron beam projections illuminating the central section of the left kidney, as exemplified in figure 1c. Each projection has 1.5×10^7 neutrons of energy 5 MeV.

The average effective dose per organ was calculated by multiplying the absorbed dose with the radiation-weighting factor 13 for neutrons at 5 MeV and the tissue weighting factor w_T for each organ obtained from ICRP 103 [11]. Based on this protocol's setup, the average effective dose was calculated summing the contribution from all organs, giving as a result 4 μSv.

From the dosimetry analysis, the average effective dose from a 10 neutron beam translations for the TOF-based NSECT is <0.1 mSv. For comparison, a typical abdominal CT exam delivers 10 mSv to average-sized adult [15].

4. CONCLUSION

A TOF-based NSECT scan was simulated with the MCNP5 code using an adult tomographic phantom containing the kidney composition for renal cell carcinoma (RCC) and healthy tissue.

The goal of this work was to demonstrate the feasibility of the TOF-based NSECT to detect and differentiate the RCC lesion from the healthy kidney tissue. We were successfully able to generate a tomographic image where a RCC lesion was identified and distinguished from the healthy kidney tissue. Due to the low sensitivity of detection of the present NSECT system,

we couldn't accurately quantify the concentration of ^{23}Na from the acquired image regarding the expected concentration for healthy kidney and RCC lesion.

From previous studies, it has been shown that it is possible to acquire several images related to different elements from a single tomographic scan [16]. We demonstrated this feature in this work by superimposing the images of ^{23}Na and ^{12}C. Therefore, the anatomy of the irradiated tissues based on the ^{12}C image and the chemical composition related to RCC lesion from the ^{23}Na image are correlated in the same image. By using two different elements, we can combine features from distinct organs and diseases. In our work, we could locate the RCC lesion within the kidney based on the concentration of ^{23}Na and ^{12}C among tissues.

It is well known in medical imaging, in order to generate a tomographic image, well sampled angular projections must be used in order to create a sinogram. Depending on the number of neutron beam projections, the NSECT scan may become unfeasible due to high dose deposition. As demonstrated in this work, the simulated TOF-based NSECT scan was able to generate a tomographic image using only 10 translations along a single angular position of the neutron beam, delivering an effective dose less than 0.1 mSv.

Additional evaluations must be carried out in order to establish the sensitivity of detection for ^{23}Na. Nevertheless, we have demonstrated the potential application of the TOF-based NSECT in detecting a RCC lesion noninvasively with a low dose to the patient.

ACKNOWLEDGMENT

REFERENCES

1. ACN. *American Cancer Society - What are the key statistics about kidney cancer?* 2013 06/04/2013]; Available from: http://www.cancer.org/cancer/kidneycancer/detailedguide/kidney-cancer-adult-key-statistics.
2. Neuzillet, Y., et al., *Accuracy and clinical role of fine needle percutaneous biopsy with computerized tomography guidance of small (less than 4.0 cm) renal masses.* J Urol, 2004. **171**(5): p. 1802-5.
3. Pandharipande, P.V., et al., *Renal mass biopsy to guide treatment decisions for small incidental renal tumors: a cost-effectiveness analysis.* Radiology, 2010. **256**(3): p. 836-46.
4. Remzi, M. and M. Marberger, *Renal tumor biopsies for evaluation of small renal tumors: why, in whom, and how?* Eur Urol, 2009. **55**(2): p. 359-67.
5. Schmidbauer, J., et al., *Diagnostic accuracy of computed tomography-guided percutaneous biopsy of renal masses.* Eur Urol, 2008. **53**(5): p. 1003-11.
6. Floyd, C.E., Jr., et al., *Introduction to neutron stimulated emission computed tomography.* Phys Med Biol, 2006. **51**(14): p. 3375-90.
7. Agasthya, G.A., et al. *Neutron time-of-flight spectroscopy for depth-resolved quantification through NSECT.* in *Nuclear Science Symposium and Medical Imaging Conference (NSS/MIC), 2011 IEEE.* 2011.

8.   X-5, *Volume I: Overview and Theory*, in *X-5 Monte Carlo Team*2003, Los Alamos National Laboratory - Report LA-UR-03-1987.

9.   Cristy, M. and F. Eckerman, *Specific Absorbed Fractions of Energy at Various Ages from Internal Photon Sources. I. Methods*, 1987, Ridge National Laboratory - Report ORNL/TM-8381/VI

10.   ICRU, *Photon, Electron, Proton and Neutron Interaction Data for Body Tissues*, 1992, International Commission on Radiation Units and Measurements - Report 46.

11.   ICRP, *Adult Reference Computational Phantoms*, 2009, International Commission on Radiological Protection - Report 103.

12.   Calvo, F.B., et al., *Variation in the distribution of trace elements in renal cell carcinoma.* Biol Trace Elem Res, 2009. **130**(2): p. 107-13.

13.   Kapadia, A.J. and J.C.E. Floyd, *An attenuation correction technique to correct for neutron and gamma attenuation in the reconstructed image of a neutron stimulated emission computed tomography (NSECT) system.* 2005: p. 737-743.

14.   Agasthya, G.A., et al., *Sensitivity analysis for liver iron measurement through neutron stimulated emission computed tomography: a Monte Carlo study in GEANT4.* Phys Med Biol, 2012. **57**(1): p. 113-26.

15.   RSNA. *Patient Safety: Radiation Dose in X-Ray and CT Exams*. RadiologyInfo.org. Developed jointly by: Radiological Society of North America (RSNA) and American College of Radiology (ACR) 2013 04/07/2013]; Available from: http://www.radiologyinfo.org/en/safety/index.cfm?pg=sfty_xray.

16.   Floyd, C.E., Jr., et al., *Neutron-stimulated emission computed tomography of a multi-element phantom.* Phys Med Biol, 2008. **53**(9): p. 2313-26.